Tension of red blood cell membrane in simple shear flow

T. Omori,[1,*] T. Ishikawa,[2] D. Barthès-Biesel,[3] A.-V. Salsac,[3] Y. Imai,[2] and T. Yamaguchi[1]
[1]*Department of Biomedical Engineering, Tohoku University, Aoba 6-6-01, Sendai, Miyagi, Japan*
[2]*Department of Bioengineering and Robotics, Tohoku University, Aoba 6-6-01, Sendai, Miyagi, Japan*
[3]*Laboratoire de Biomécanique et Bioingénierie (UMR CNRS 6600), Université de Technologie de Compiègne, 60205 Compiègne, France*
(Received 7 June 2012; revised manuscript received 7 October 2012; published 29 November 2012)

When a red blood cell (RBC) is subjected to an external flow, it is deformed by the hydrodynamic forces acting on its membrane. The resulting elastic tensions in the membrane play a key role in mechanotransduction and govern its rupture in the case of hemolysis. In this study, we analyze the motion and deformation of an RBC in a simple shear flow and the resulting elastic tensions on the membrane. The large deformation of the red blood cell is modelled by coupling a finite element method to solve the membrane mechanics and a boundary element method to solve the flows of the internal and external liquids. Depending on the capillary number Ca, ratio of the viscous to elastic forces, we observe three kinds of RBC motion: tumbling at low Ca, swinging at larger Ca, and breathing at the transitions. In the swinging regime, the region of the high principal tensions periodically oscillates, whereas that of the high isotropic tensions is almost unchanged. Due to the strain-hardening property of the membrane, the deformation is limited but the membrane tension increases monotonically with the capillary number. We have quantitatively compared our numerical results with former experimental results. It indicates that a membrane isotropic tension $\mathcal{O}(10^{-6}$ N/m) is high enough for molecular release from RBCs and that the typical maximum membrane principal tension for haemolysis would be $\mathcal{O}(10^{-4}$ N/m). These findings are useful to clarify not only the membrane rupture but also the mechanotransduction of RBCs.

DOI: 10.1103/PhysRevE.86.056321 PACS number(s): 47.63.−b, 83.50.−v, 87.16.D−, 46.15.−x

I. INTRODUCTION

Under physiological conditions, a healthy human red blood cell (RBC) has the resting shape of a biconcave disk. Its membrane encloses a Newtonian haemoglobin solution. It consists primarily of a phospholipid bilayer and an elastic spectrin network. The lipid bilayer strongly resists local surface area changes, but the elasticity of the cytoskeleton enables the RBCs to undergo large extensional deformation while maintaining the structural integrity of the membrane.

Flow-induced RBC deformation affects the cell ability to release various molecules and regulate their concentrations in blood [1]. In particular, when RBCs are strongly deformed by the surrounding fluid flow, they release ATP and ADP [2,3]. ATP is a well-known energy source for intracellular functions, and extracellular ATP plays an important role as a signaling molecule in a variety of physiological processes [3]. In addition, ADP is a known factor in the primary aggregation of platelets [2]. Flow-induced deformation may also lead to RBC rupture, called haemolysis. There is no doubt that a causal relationship between the stress level in the membrane and haemolysis exists. Thus, clarification of the stresses in the membrane is crucial towards understanding the physiology and pathology of microcirculation. As the RBC membrane is very thin, only the deformation of its median surface is considered. Henceforth, the term "membrane" refers to the two-dimensional median surface. In the membrane model, the stresses are integrated across the wall thickness and replaced by tensions, i.e., forces per unit length of the median deformed surface.

The motion and deformation of capsules and vesicles in shear flow have been investigated by a number of researchers [4–11]. In the low shear rate regime, a nonspherical capsule rotates like a rigid body, yielding a large amplitude oscillation of the inclination angle. This motion, called tumbling motion, has been observed in studies of capsule [10], vesicle [5], and red blood cell [12]. At high shear rate, the membrane rotates around the capsule shape. The inclination angle and the deformed shape periodically oscillate: this is the so-called swinging motion. The swinging-tumbling transition of capsules and vesicles was also investigated analytically [5,8,9] and numerically [10,13]. In the case of an RBC, two different kinds of motion were discussed in Skotheim and Secomb [8] and Vlahovska *et al.* [9]. One is the breathing motion, which is defined by large shape oscillations and a swinging motion at the transition regime [9,11]. The other is the intermittent motion, which is analytically predicted by Skotheim and Secomb [8]. In this motion, swinging is periodically interrupted by a tumbling motion.

Ramanujan and Pozrikidis [7] reported the first three-dimensional computation of an RBC in simple shear flow. The RBC is modelled as a capsule with a hyperelastic membrane and the cell reference shape is assumed to be a biconcave disk. The nonspherical reference shape leads to anisotropic membrane properties and yields a periodic shape oscillation during the tank-treading motion. In their study, however, stable long computational times are not achieved because of numerical instabilities and only limited results are hence discussed in the paper. Le *et al.* [4] also compared the motion and deformation of a biconcave disk with those of an oblate capsule in simple shear flow using an immersed boundary method; however, only few results with nonidentical viscosity ratio are reported. Thus, further analyses with various viscosity ratios and shear rates are needed in order to fully understand the kinematics of an RBC in fluid flow. No study has either thoroughly examined the elastic tensions of the membrane despite its relevance in understanding RBC physiology and pathologies. Only Pozrikidis [6] investigated the tension on the RBC

*omori@pfsl.mech.tohoku.ac.jp

membrane in the tumbling regime. He found that compressive tensions appeared on the membrane already at low capillary numbers, but did not investigate RBCs under higher values.

To rigorously investigate membrane tensions, the fluid-structure interaction between the internal or external flows and the membrane has to be accurately solved. Based on the small size of the RBC, it is usually assumed that the fluid velocity field around a RBC is governed by the Stokes equation, which can be expressed in terms of surface integrals defined on the cell membrane. This approach, known as the boundary element method [10,14], treats the discontinuity of the hydrodynamic stress tensor across the membrane explicitly and is thus very accurate. Walter *et al.* [10] solved shear-induced capsule deformation using the boundary element method coupled with the finite element method for membrane mechanics, which was shown to be very advantageous with respect to numerical stability. The numerical method was then generalized by Foessel *et al.* [15] to take into account the effect of a viscosity contrast between the internal and external liquids.

In this study, we use the method of Foessel *et al.* [15] and apply it to a single RBC in a simple shear flow. We specifically investigate the mechanical tensions that arise in the membrane. In Sec. III A, we compute the kinematics of an RBC subjected to different flow strengths and viscosity ratios. We then investigate in detail the effects of the capillary number and viscosity ratio on the membrane tension in Sec. III C. In Sec. IV, we discuss the results and bring conclusions to our study.

II. MECHANICS OF AN RBC IN SIMPLE SHEAR FLOW

We consider the dynamics of an RBC subjected to a simple shear flow. The RBC is modelled as a capsule with a hyperelastic membrane with surface shear elastic modulus G_s and area dilation modulus K_s. The motion of a capsule in flow can now be considered as a classical problem, which is only briefly explained here (more details can be found in [14,16]).

A. Problem statement

1. Fluid mechancis

We assume that the RBC is filled with an incompressible Newtonian fluid with density ρ and viscosity $\lambda\mu$. It is freely suspended in another fluid with the same density ρ but viscosity μ. Due to the small size of an RBC, the inertial effects of the internal and external fluid flows are small compared to viscous effects, so that the fluid flows are governed by the Stokes equation. The velocity field $\boldsymbol{v}$ can be written as an integral equation over the instantaneous deformed membrane surface S [14],

$$\boldsymbol{v}(\boldsymbol{x}) = \frac{2}{1+\lambda}\boldsymbol{v}^{\infty}(\boldsymbol{x}) - \frac{1}{4\pi\mu(1+\lambda)} \times \int_S \boldsymbol{J}(\boldsymbol{x},\boldsymbol{y}) \cdot [\boldsymbol{\sigma}_{\text{out}}(\boldsymbol{y}) - \boldsymbol{\sigma}_{\text{in}}(\boldsymbol{y})] \cdot \boldsymbol{n}(\boldsymbol{y}) dS + \frac{1-\lambda}{4\pi(1+\lambda)} \int_S \boldsymbol{v}(\boldsymbol{y}) \cdot \boldsymbol{K}(\boldsymbol{x},\boldsymbol{y}) \cdot \boldsymbol{n}(\boldsymbol{y}) dS, \quad (1)$$

where $\boldsymbol{v}^{\infty}$ is an undisturbed background flow, λ is the viscosity ratio between the internal and external liquids, $\boldsymbol{n}$ is the outward unit normal vector on the surface, $\boldsymbol{J}$ and $\boldsymbol{K}$ are the Green's functions of the single- and double-layer potentials, and $\boldsymbol{\sigma}_{\text{in}}$ and $\boldsymbol{\sigma}_{\text{out}}$ are viscous fluid stress of the internal and external liquids, respectively. The dynamic condition requires that the load $\boldsymbol{q}$ exerted on the membrane must be equal to the viscous jump across the thin membrane,

$$[\boldsymbol{\sigma}_{\text{out}} - \boldsymbol{\sigma}_{\text{in}}] \cdot \boldsymbol{n} = \boldsymbol{q}.$$

2. Membrane mechancis

Since the thickness of the RBC membrane is small compared with the cell size and curvature radius, the membrane can be modelled as a two-dimensional hyperelastic surface S (the median surface) devoid of bending resistance [17]. Skalak *et al.* [18] introduced a law (SK) to model the large deformation of an RBC membrane. The strain energy w and principal tensions in the membrane τ_1 and τ_2 ($\tau_1 \geqslant \tau_2$) of the SK law are given by

$$w = \frac{G_s}{4}\left[\lambda_1^4 + \lambda_2^4 - 2\lambda_1^2 - 2\lambda_2^2 + 2 + C\left(\lambda_1^2\lambda_2^2 - 1\right)^2\right], \quad (2)$$

and

$$\tau_1 = \frac{G_s\lambda_1}{\lambda_2}\left[\lambda_1^2 - 1 + C\lambda_2^2\left(\lambda_1^2\lambda_2^2 - 1\right)\right] \quad \text{(likewise for } \tau_2\text{)}, \quad (3)$$

where λ_1,λ_2 are the two principal in-plane stretch ratios and C is a dimensionless material coefficient that measures the resistance to area dilation. The area dilation modulus of the SK law is $K_s = G_s(1+2C)$ [17]. By setting a large value of C, one can express the area-incompressibility of the membrane. Walter *et al.* [10] investigated the effects of C on the deformation of an ellipsoidal capsule in a simple shear flow and showed that $C = 10$ is high enough to express the area incompressibility of the membrane within 1%. Accordingly, all of the results presented herein correspond to $C = 10$.

Negligible inertia of the membrane deformation, the motion of the membrane is governed by the local equilibrium equation [14]

$$\nabla_s \cdot \boldsymbol{\tau} + \boldsymbol{q} = \boldsymbol{0}, \quad (4)$$

where ∇_s is the surface divergence operator. The above equilibrium equation can be written in a weak form using the virtual work principle [10]

$$\int_S \hat{\boldsymbol{u}} \cdot \boldsymbol{q}\, dS = \int_S \hat{\boldsymbol{\varepsilon}} : \boldsymbol{\tau}\, dS, \quad (5)$$

where $\hat{\boldsymbol{u}}$ and $\hat{\boldsymbol{\varepsilon}} = \frac{1}{2}(\nabla_s\hat{\boldsymbol{u}} + \nabla_s\hat{\boldsymbol{u}}^T)$ are the virtual displacement and strain, respectively.

B. Numerical methods

We track the Lagrangian position of the membrane material points over time and can thus readily compute the local membrane deformation, and principal stretch ratios λ_1,λ_2. The in-plane elastic tensions $\boldsymbol{\tau}$ are obtained from the membrane constitutive law. The finite element method [10,14] is used to solve Eq. (5) and calculate the viscous load $\boldsymbol{q}$ for a given membrane deformation. Equation (1) is solved by a boundary element method [10,15]. Once the velocity field

$\boldsymbol{v}$ is computed, the membrane material point $\boldsymbol{x}$ is updated by means of the kinematic condition $\partial \boldsymbol{x}/\partial t = \boldsymbol{v}(\boldsymbol{x},t)$, which guarantees continuity between the membrane velocity and the internal or external fluid velocity. The above equation is solved using an explicit second-order Runge-Kutta method. The whole process is repeated until steady periodic motion is achieved. For details of the numerical methods, please refer to our former studies [15,19].

C. Reference shape and numerical conditions

In a Cartesian reference frame with the RBC center as origin, the undisturbed velocity field $\boldsymbol{v}^{\infty}$ of the external fluid is given by

$$v_1^{\infty} = \dot{\gamma} x_2, \quad v_2^{\infty} = v_3^{\infty} = 0, \tag{6}$$

where $\dot{\gamma}$ is the shear rate. The RBC deformation depends on the viscosity ratio λ and on the capillary number $\mathrm{Ca} = \mu\dot{\gamma}\ell/G_s$, which measures the ratio between the viscous and elastic forces. The parameter ℓ is the radius of the sphere with the same volume as the cell.

To discretize the RBC membrane, we use a subdividing method similar to the one described in [10]. A first mesh is constructed by means of an icosahedron with 20 regular triangles inscribed on a sphere with radius ℓ. A new computational node is placed at the middle of each edge so that each triangle element is divided into four new elements. The new nodes are projected onto the sphere and the procedure is repeated until the desired number of elements is reached. We thus obtain a mesh with node points X_i in a coordinate system centered on the cell center. These node points are then projected to position X_i^{rbc} on the biconcave axisymmetric RBC profile given by [20] by means of the following transformation:

$$\begin{aligned} X_1^{\mathrm{rbc}} &= \frac{R_0}{\ell} X_1, \\ X_2^{\mathrm{rbc}} &= \pm\frac{1}{2} R_0 (1-r^2)^{1/2}(C_0 + C_2 r^2 + C_4 r^4), \\ X_3^{\mathrm{rbc}} &= \frac{R_0}{\ell} X_3, \end{aligned} \tag{7}$$

where $r^2 = (X_1^2 + X_3^2)/\ell^2$ and R_0 is the radius of the biconcave disk [Fig. 1(a)]. The plus sign in the second term is for $X_2 > 0$ (likewise for minus sign). Under physiological conditions, the shape parameters C_0, C_2, C_4 and radius R_0 of an RBC are given by [20] $C_0 = 0.21$, $C_2 = 2.0$, $C_4 = -1.12$, and $R_0/\ell = 1.39$. The RBC membrane has a shape memory [21], but the question of whether or not the biconcave disk shape of the RBC is stress free is still under debate. Since the question is not yet resolved, we have assumed the stress-free reference shape to be the biconcave disk.

At time $t = 0$, the cell is positioned with its X_2 axis in the shear plane, where it remains, in view of the symmetry of the problem and of the Stokes equations. We use this specific initial orientation so as to easily compare our numerical results with former studies, which also use the same initial orientation, though we recently reported its effect on the RBC behavior [19]. The inclination angle β, which is defined as the angle between the major axis and the flow direction, is thus initially set to 0. The angle α is defined as the angle between a material point P and the flow direction [cf. Fig. 1(b)]. The material point P is initially located at $(x_1,x_2,x_3) = (R_0,0,0)$.

The motion and deformation of the cell are conveniently described by the Taylor parameter D_{12} defined as

$$D_{12} = \frac{|L_1 - L_2|}{L_1 + L_2}, \tag{8}$$

where L_1, L_2 are the semiaxis length of the ellipsoid of inertia of the deformed capsule in the 12 plane. Due to the nonspherical shape of the biconcave disk, the initial value D_{12}^0 of the Taylor parameter is $D_{12}^0 = 0.51$.

As the viscosity ratio λ increases, the computation tends to become unstable because membrane compression increases. In particular when $\lambda > 3$, the membrane is significantly crumpled and the computation diverges before reaching a steady periodic motion. In order to ensure both numerical accuracy and stability, the parametric range of λ is set from 1 to 3 in this study.

For the purposes of numerical accuracy and stability of the coupling algorithm, the nondimensional time step $\dot{\gamma}\Delta t$ must be sufficiently small. In this study, $\dot{\gamma}\Delta t$ is set in the range 5.0×10^{-6}–5.0×10^{-3} to guarantee time convergence. We also investigated mesh convergence of the numerical method by calculating deformations of a spherical capsule in shear flow. The deformation is measured by the Taylor parameter D_{12}. The results obtained by 5120 and 20 480 linear triangle elements differ less than 0.1% ($\mathrm{Ca} = 1, \lambda = 1, C = 1$). We thus

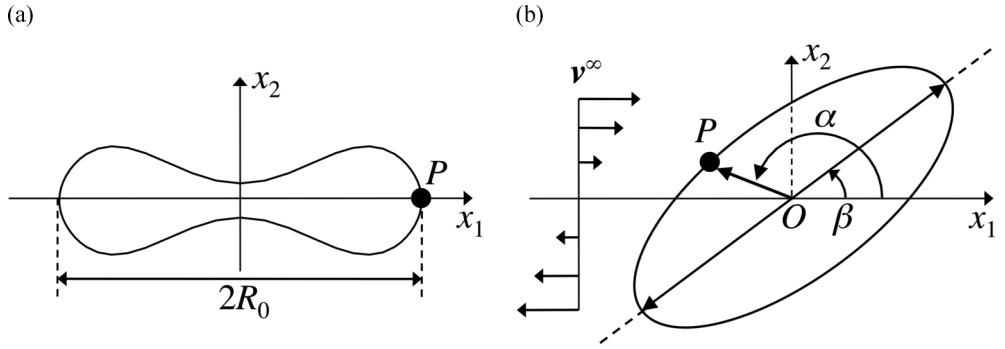

FIG. 1. (a) Initial shape of the RBC in the shear plane. R_0 is the radius of a biconcave disk. (b) Schematic illustration of deformed RBC. The inclination angle β is defined as the angle between the major axis and the flow direction. The angle α is defined as the rotational angle of the material point P on the membrane, which is initially located at $(x_1,x_2,x_3) = (R_0,0,0)$.

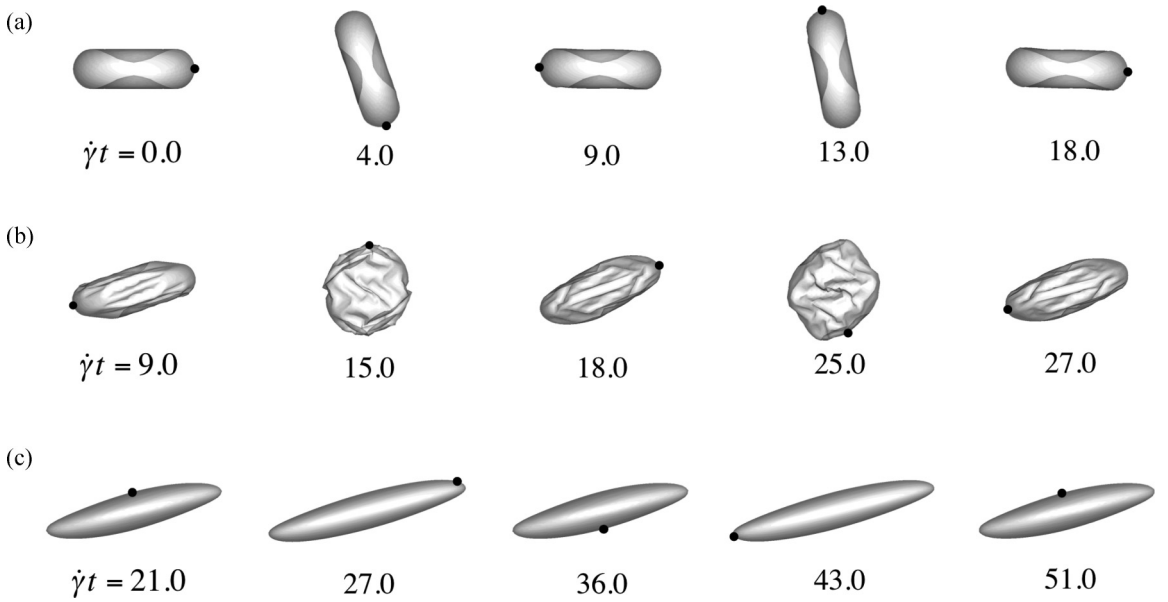

FIG. 2. Time sequences of the RBC shape in the shear plane during a tank-treading period with (a) Ca = 0.002, (b) 0.02, and (c) 3.0. For all cases, the viscosity ratio $\lambda = 1.0$. A black dot represents a material point of the membrane, which is initially located on $x_1 = R_0$, $x_2 = x_3 = 0$. The nondimensional time $\dot{\gamma}t$ is given below each shape.

decided to use 5120 linear triangles for the computation in this study.

III. RESULTS AND DISCUSSIONS

A. Kinematics of an RBC in simple shear flow

In this section, we investigate the kinematic motion and deformation of the RBC in simple shear flow with various capillary numbers Ca and viscosity ratio λ conditions. Successive profiles of the deformed RBC during a tank-treading period at steady state with Ca = 0.002, 0.02, and 3.0 are shown in Fig. 2 for $\lambda = 1$. At low capillary number [Ca = 0.002, Fig. 2(a)], the RBC rotates like a quasirigid body. This motion corresponds to the tumbling regime, which has been evidenced for both capsules and vesicles [5,9,10]. At high capillary number [Ca = 3.0, Fig. 2(c)], the RBC shows a tank-treading motion with a steady inclination angle. Due to the anisotropic reference shape, the inclination angle periodically oscillates around the mean angle with small amplitude oscillation [cf. Fig. 3(b)]. This type of cell motion, referred to as swinging, has been reported in previous experimental [12] and numerical studies [4,7] of an RBC in shear flow. The point in Fig. 2(c) shows the successive positions of a membrane material point so that the tank-treading motion thus appears clearly. For Ca = 0.02 [Fig. 2(b)], the RBC is subjected to compressive stress leading to the wrinkling of the membrane. Since the membrane is described by a membrane model devoid of bending stiffness, the configuration of the actual physical wrinkles cannot be predicted. The amplitude and number of the wrinkles that we obtain depend only on the mesh. However, their location is well predicted by the model. Since precise and robust numerical models accounting for bending effects

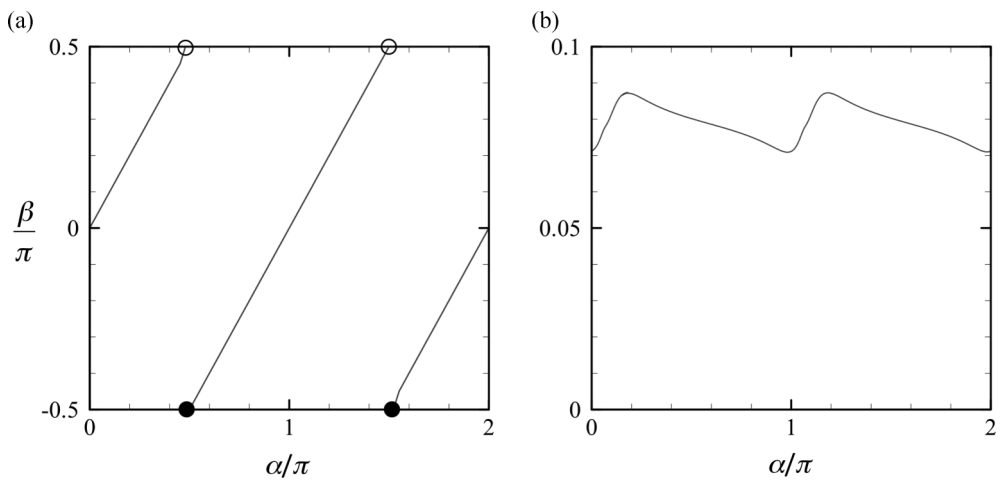

FIG. 3. Inclination angle of the RBC during a period: (a) Ca = 0.002, and (b) Ca = 3.0. Numerical conditions are the same as those of Fig. 2.

are still to be developed, it is not possible at this stage to know to which extent the average shape of the capsule is affected by the presence of the folds.

In the tumbling-to-swinging transition, the RBC shows a large shape oscillation from circular to elliptic shape, as shown in Fig. 2(b). This large-amplitude shape oscillation at the transition threshold is called the breathing motion [11] and is found in former studies of capsules [9–11,13,22] and vesicles [5]. The transition behavior from tumbling to swinging of nonspherical capsules has been investigated by several researchers. Skotheim and Secomb [8] analytically investigated the transition of an RBC in shear flow and first reported the intermittent behavior (swinging periodically interrupted by a tumble) of the RBC at the transition. However, this intermittent motion of the RBC has not been directly observed in former experimental studies. Vlahovska *et al.* [9] also analytically investigated the tumbling-swinging transition of the RBC. They found that the intermittent behaviour occurs only when the RBC deforms in the shear plane and does not undergo stretching or compression along the vorticity direction. When the RBC deforms also along the vorticity direction, it shows a breathing motion in the transition regime. Our results are consistent with the results of Vlahovska *et al.* [9]. In particular here also no intermittent behavior is found since our capsule is free to undergo breathing.

To investigate the kinematics of an RBC in more detail, the time evolution of the Taylor parameter D_{12} is shown in Fig. 4. In the tumbling regime (Ca = 0.002), the RBC rotates like a rigid body. Thus, D_{12} does not change markedly throughout the entire range of computational time. When the RBC has a swinging motion (Ca = 3.0), D_{12} oscillates periodically and the frequency is twice as large as the tank-treading motion, due to the initial symmetry of the RBC profile. In the tumbling-to-swinging transition (Ca = 0.02), we observe large amplitude oscillations and small values of D_{12}. This is because the RBC shape periodically changes from ellipsoidal to quasicircular, and the quasicircular profile corresponds to $D_{12} \cong 0$.

In most studies of vesicles and capsules, the kinematic motion is characterized by the inclination angle. In the swinging motion, the average angle is finite, but the amplitude of oscillation is small. As one approaches the tumbling regime, the amplitude of angle oscillation increases, which is the breathing mode [5]. The inclination angle shows a clear contrast between the tumbling motion and the swinging motion, as shown in Fig. 3. However, this parameter may not be appropriate to define the breathing mode. In the breathing regime, the capsule shape becomes quasicircular, which makes it difficult to identify the long axis and leads to large numerical errors when estimating the critical capillary number Ca* at the transition. Furthermore, we believe that the transition occurs continuously in the parameter space of Ca and cannot be identified by a specific value of Ca*. To overcome the above difficulties, Walter *et al.* [10] used a transition criterion based on the minimum value of the Taylor parameter. Indeed in the transition regime, the value of the Taylor parameter becomes small, as shown in Fig. 4. We can therefore define the transition regime by studying the minimum value of the Taylor parameter min D_{12} as a function of Ca and λ, as shown in Fig. 5. It is clear that min D_{12} becomes small for all $\lambda \leqslant 3$ cases. Thus, to determine the interval of the critical capillary number Ca*, we define a transition criterion as min $D_{12} \leqslant 0.1$. This threshold value corresponds to a relative difference of 20% between L_1 and L_2. We note that the range of Ca* is not sensitive to selection of the threshold value if we choose sufficiently small values of the threshold in min D_{12}, because the deformation changes rapidly in the transition regime as shown in Fig. 5. The sharp transition indicates the sudden change from tumbling to swinging motion of the RBC. This tendency is consistent with former studies [9,10]. The sharp transition also induces the difficulty to detect the critical capillary number Ca* in experimental observations, because the narrow parameter range may be hard to control experimentally. The values of Ca* increases with λ as shown in Table I. For a high viscosity ratio, the deformation of the RBC tends to be suppressed because the effect of the inner viscosity becomes significant. As a result, the tumbling regime extends to higher Ca values and Ca* increases as λ increases.

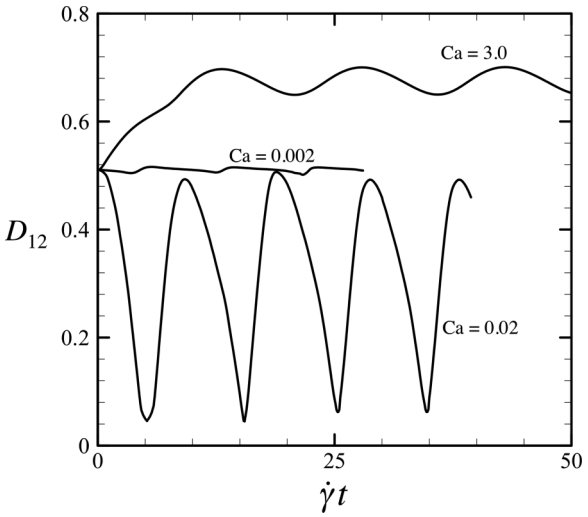

FIG. 4. Time change of Taylor parameter D_{12} with Ca = 0.002, 0.02, and 3.0.

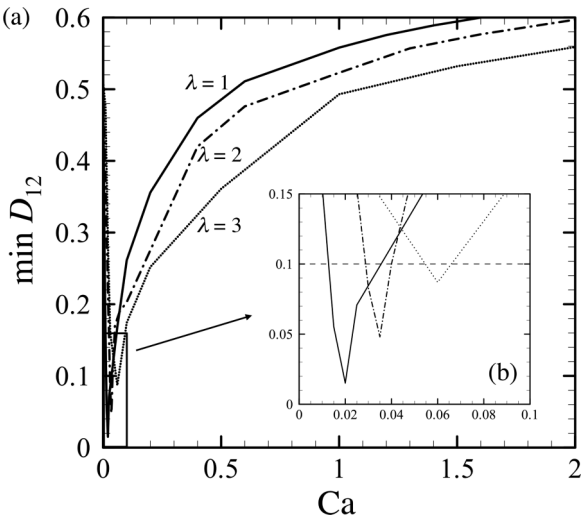

FIG. 5. Minimum Taylor parameter during a periodic motion with λ = 1, 2, and 3. Zoom view in low Ca regime is shown in (b). The broken line in the figures indicates min $D_{12} = 0.1$.

TABLE I. Interval of critical capillary number Ca^*.

$\gamma = 1$	$Ca^* \in [0.013, 0.036]$
$\gamma = 2$	$Ca^* \in [0.029, 0.04]$
$\gamma = 3$	$Ca^* \in [0.055, 0.066]$

B. Cell deformation

We investigate the RBC deformation with various Ca and λ. Flow-induced deformation directly correlates to the membrane tension, so that knowledge of the deformation can be used to estimate the membrane tension in shear flow. The maximum and averaged longest axis length calculated over one period are shown in Figs. 6(a) and 6(b), respectively. The RBC gradually elongates in the flow direction as Ca increases. The slope becomes smaller with Ca, because the membrane is modelled by the SK law, which is strain hardening and thus opposes large deformation. The deformation also tends to be suppressed when the viscous effects inside the capsule become large, i.e., for high values of λ. These results suggest that not only the shear rate, but also the viscosity ratio of the internal and external liquids, influences the deformation of the RBC in shear flow.

C. Membrane tension under shear flow

The membrane tension level can be used to predict the rupture and mechanotransduction of RBCs. We thus investigate the largest in-plane principal tensions τ_i ($\tau_1 \geqslant \tau_2$) and the isotropic tension τ^p in the membrane of the RBC. In the case of a two-dimensional (2D) isotropic elastic membrane, the isotropic membrane tension can be calculated by $\tau^p = (\tau_1 + \tau_2)/2$.

In Fig. 7(a), distributions of the elastic strain energy w in the shear plane during a tank-treading period are shown (Ca = 3 and $\lambda = 1$). The w distribution changes periodically together with the shape oscillation. Accordingly, the principal tension τ_1 oscillates periodically [Fig. 7(b)]. When the RBC is most elongated along the flow direction ($\dot{\gamma}t = 27.0, 43.0$ in the figure), high values of τ_1 appear on the plane perpendicular to the minor axis of the deformed RBC. When the RBC is most elongated along the x_3 direction ($\dot{\gamma}t = 21.0$, 36.0, and 51.0), however, τ_1 becomes highest on the plane perpendicular to the x_3 axis, which is the maximum value during the period. In the case of a hyperelastic membrane, high values of the principal tension should correlate with the yield tension of the material, i.e., the tolerated maximum elastic tension. Thus, these results regarding the high τ_1 region may be important for understanding the haemolysis mechanism.

Recently, several researchers have worked on the mechanotransduction of biological cells [2,3,23]. Yoshimura *et al.* [23] reported that the mechanosensitive ion channel MscL found in *Escherichia coli* cells is opened by isotropic tension τ^p. Though the ion channel structures of an RBC membrane are more complicated than those of bacteria, the isotropic tensions likely play an important role in the regulation of ion channels. The distribution of τ^p is also shown in Fig. 7(c). High values of τ^p appear only on the plane perpendicular to the minor axis of the deformed RBC, though the region of the high principal tension periodically oscillates. Thus, the distributions of τ_1 and τ^p are qualitatively different in the RBC in shear flow.

We define the maximum principal tension as

$$\max \tau_1 = \max_t [\max_{\boldsymbol{x}} \tau_1(\boldsymbol{x}, t)], \tag{9}$$

where $\max_t$ indicates the maximum value in one tank-treading period and $\max_{\boldsymbol{x}}$ indicates the maximum value on the membrane. The values of $\max \tau_1$ as a function of Ca and λ are shown in Fig. 8. This figure clearly shows a linear relationship between the maximum tension and the capillary number. When Ca is invariant, the maximum tension tends to be larger as λ decreases. To see the relationship between the tension and deformation, the maximum tension as a function of the long axis length L_1 is also shown in Fig. 9. We see that the strain-hardening behavior of the RBC is due to the nonlinearity of the SK law.

Next, we calculate the instantaneous maximum isotropic tension $\max \tau^p$, which may be considered as the criterion for the opening of the mechanosensitive ion channel (see Fig. 10). We also calculate the averaged value of τ^p by using

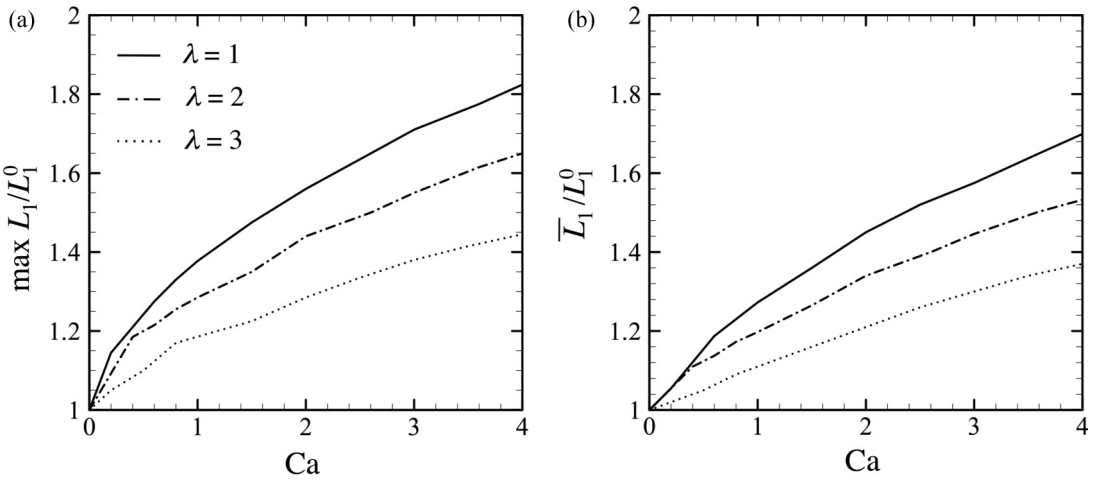

FIG. 6. (a) Maximum and (b) time average values of the long axis L_1. L_1^0 is the initial length of L_1.

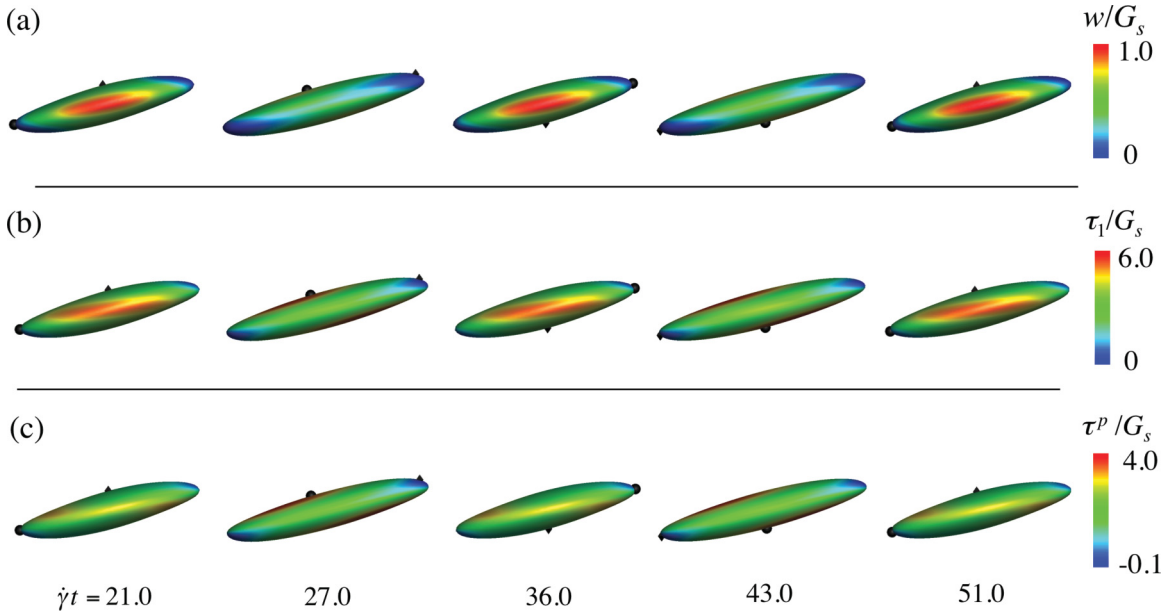

FIG. 7. (Color) Distributions of (a) the elastic energy function w, (b) in-plain elastic principal tension τ_1, and (c) the isotropic membrane tension τ^p. Diamond and dot on the membrane indicate material points of the membrane, which are initially located on the major and revolution axes, respectively.

the equation

$$\bar{\tau}^p = \frac{1}{ST}\int_T \int_S \tau^p(\boldsymbol{x},t)dSdt, \tag{10}$$

where S is the surface area of the membrane and T is the period of tank-treading motion.

Since the molecular release due to the RBC deformation may be proportional to the time of channel opening and the number of open channels, $\bar{\tau}^p$ may correlate with the total amount of molecules released from the RBC. We again observe the almost linear relationships between max τ^p and Ca as well as $\bar{\tau}^p$ and Ca. Wan *et al.* [3] investigated shear-induced release of ATP from RBCs using a microfluidic channel. They reported that the amount of released ATP increased linearly with the shear rate. Since $\bar{\tau}^p$ increases linearly with the shear rate as shown in Fig. 8(b), this suggests that the mechanotransduction reported by Wan *et al.* might also be regulated by the isotropic tension on the membrane.

We now quantitatively compare our numerical results with experimental data of the literature. The shear elastic modulus G_s of an RBC membrane is estimated in recent optical tweezer experiments to be $G_s = 1$–22 μN/m [24]. The range of the value is strongly dependent on the selection of constitutive laws. In the case of strain-hardening laws, such as the SK law, it is commonly estimated to be $G_s \cong 4$–5 μN/m [25].

Using $G_s = 4$ μN/m, we first analyze the results of isotropic tension τ^p. Wan *et al.* [3] investigated shear-induced release of ATP from RBCs using a microfluidic channel. In

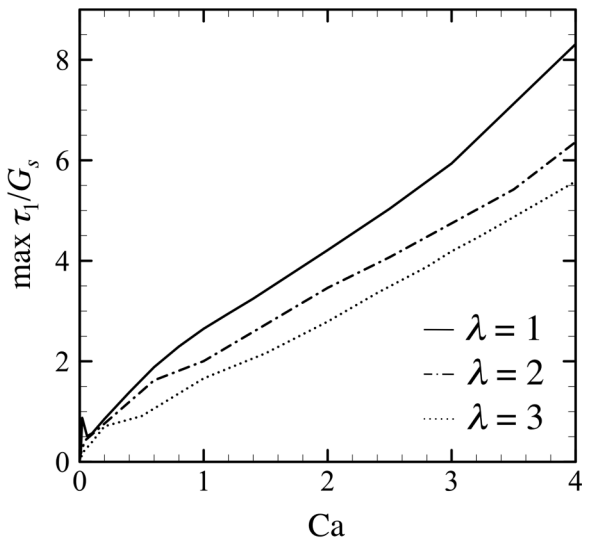

FIG. 8. Maximum principal tension during a tank-treading period as a function of Ca with $\lambda = 1$, 2, and 3.

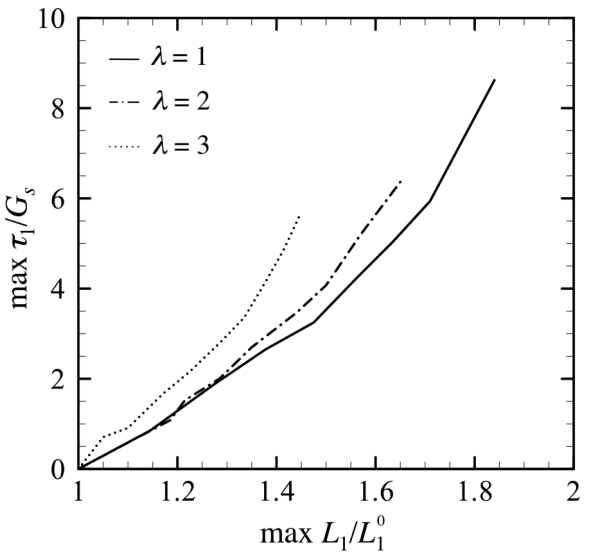

FIG. 9. Maximum principal tension as a function of the deformation of RBC.

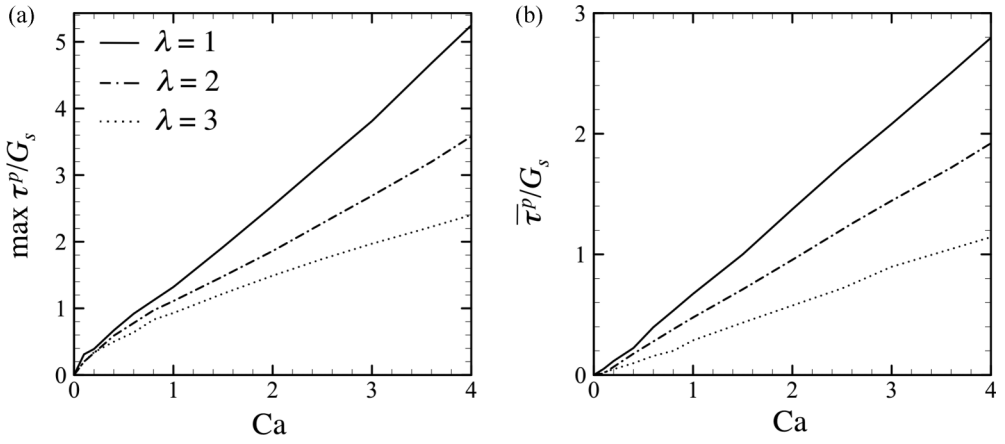

FIG. 10. (a) Maximum isotropic tension and (b) averaged τ^p as a function of Ca with $\lambda = 1$, 2, and 3.

their experiment, the average fluid shear stress is controlled from 0.4 to 3.3 Pa. When we assume the characteristic length to be equal to $\ell = 2.82\ \mu$m [20], Wan's experimental condition is equivalent to Ca = 0.3–2.3. In this Ca regime, the average isotropic tension during a tank-treading period $\bar{\tau}^p$ is estimated to be 0.7–6.4 μN/m ($\lambda = 1$), 0.5–4.4 μN/m ($\lambda = 2$), and 0.3–2.6 μN/m ($\lambda = 3$) [cf. Fig. 8(b)]. These results indicate that $\bar{\tau}^p = 1\ \mu$N/m is high enough to induce molecular release from RBCs. In the case of *E. coli* cells, on the other hand, the mechanosensitive calcium ion channel was activated by 5–10 kPa stress exerted by micropipette aspiration [23]. These results clearly illustrate that the threshold value to open the mechanosensitive channels is completely different between RBCs and *E. coli*. Thus, detailed analysis about membrane tension is needed to better understand the molecular release from RBCs. Our results on the isotropic tension can provide information on the mechanotransduction phenomena in the RBC.

Haemolysis is one of the biggest problems in the research field of artificial organs. Due to the nonphysiological fluid stress levels in artificial organs, RBCs are often destroyed. Many researchers have investigated the correlation between the applied fluid shear stress and RBC membrane rupture. The threshold value is now believed to be on the order of 100 Pa in plasma solution [26]. If we again assume a length scale $\ell = 2.82\ \mu$m, shear stress of 100 Pa is estimated to Ca = 70. This is beyond the stable region of our computation and we therefore cannot obtain the results of the maximum tension on the membrane in this range. But if the maximum principal tension (cf. Fig. 8) increases linearly to Ca = 70, the maximum tension would be about 4×10^{-4} N/m ($\lambda = 3$) to 6×10^{-4} N/m ($\lambda = 1$). In microcirculation, the average shear rate can be estimated to be several hundreds (1/s) [27], which corresponds to a capillary number of the order of 10^{-1}. It can reach larger values (a few thousands 1/s) in blood vessels with complex geometries (e.g., when flowing into the pores of the spleen). But in all cases, the typical capillary number remains much smaller than Ca = 70, so that lysis is unlikely to occur in the microcirculation.

IV. CONCLUSION

In this study, we investigated the kinematic motion of the RBC in simple shear flow. Three types of motion are observed: tumbling motion, swinging motion, and transition. We also investigated RBC deformation. The RBC gradually elongates towards the flow direction as Ca increases, but the deformation is saturated in the high Ca regime due to the strain-hardening property of the membrane.

In Sec. III C, we investigated the principal and isotropic tension that appear on the RBC membrane. Principal tension distributions change periodically together with the shape oscillation, and the maximum tensions appear on the shear plane. The high isotropic tension, however, appears only at the plane perpendicular to the minor axis of the deformed RBC. We also investigated the maximum principal tension and isotropic tension on the membrane. These tensions increase monotonically with Ca even though the deformation is suppressed in the high Ca regime. Last, we compare our numerical results with former experimental results, and quantitatively discussed about the threshold of tension for ATP release and for haemolysis. These membrane tension findings may be useful to better understand the mechanisms of haemolysis and mechanotransduction of RBCs.

ACKNOWLEDGMENTS

This work was supported by the Conseil Régional de Picardie (MODCAP grant) and by the French Ministère de la Recherche (Pilcam2 grant).

[1] H. L. Goldsmith, D. N. Bell, and S. Braovac, Biophys. J. **69**, 1584 (1995).
[2] T. M. Alkhamis, R. L. Beissinger, and J. R. Chediak, Blood **75**, 1568 (1990).
[3] J. Wan, W. D. Ristenpart, and H. A. Stone, Proc. Natl. Acad. Sci. USA **105**, 16432 (2008).
[4] D. V. Le and Z. Tan, J. Comput. Phys. **229**, 4097 (2010).
[5] C. Misbah, Phys. Rev. Lett. **96**, 028104 (2006).

[6] C. Pozrikidis, Ann. Biomed. Eng. **31**, 1194 (2003).
[7] S. Ramanujan and C. Pozrikidis, J. Fluid Mech. **361**, 117 (1998).
[8] J. M. Skotheim and T. W. Secomb, Phys. Rev. Lett. **98**, 078301 (2007).
[9] P. M. Vlahovska, Y. N. Young, G. Danker, and C. Misbah, J. Fluid Mech. **678**, 221 (2011).
[10] J. Walter, A.-V. Salsac, and D. Barthès-Biesel, J. Fluid Mech. **676**, 318 (2011).
[11] A. Z. K. Yazdani and P. Bagchi, Phys. Rev. E **84**, 026314 (2011).
[12] M. Abkarian, M. Faivre, and A. Viallat, Phys. Rev. Lett. **98**, 188302 (2007).
[13] S. Kessler, R. Finken, and U. Seifert, J. Fluid Mech. **605**, 207 (2008).
[14] D. Barthès-Biesel, J. Walter, and A.-V. Salsac, *Flow-induced Deformation of Artificial Capsules* (Taylor & Francis, London, 2010), pp. 35–70.
[15] E. Foessel, J. Walter, A.-V. Salsac, and D. Barthès-Biesel, J. Fluid Mech. **672**, 477 (2011).
[16] D. Barthès-Biesel and J. M. Rallison, J. Fluid Mech. **113**, 251 (1981).
[17] D. Barthès-Biesel, A. Diaz, and E. Dhenin, J. Fluid Mech. **460**, 211 (2002).
[18] R. Skalak, A. Tozeren, R. P. Zarda, and S. Chien, Biophys. J. **13**, 245 (1973).
[19] T. Omori, Y. Imai, T. Yamaguchi, and T. Ishikawa, Phys. Rev. Lett. **108**, 138102 (2012).
[20] E. A. Evans and Y. C. Fung, Microvasc. Res. **4**, 335 (1972).
[21] T. M. Fischer, Biophys. J. **86**, 3304 (2004).
[22] R. Finken, S. Kessler, and U. Seifert, J. Phys.: Condens. Matter **23**, 184113 (2011).
[23] K. Yoshimura, J. Usukura, and M. Sokabe, Proc. Natl. Acad. Sci. USA **105**, 4033 (2008).
[24] S. Suresh, J. Mater. Res. **21**, 1871 (2006).
[25] R. M. Hochmuth and R. E. Waugh, Annu. Rev. Physiol. **49**, 209 (1987).
[26] L. B. Levertt, J. D. Hellums, C. P. Alfrey, and E. C. Lynch, Biophys. J. **12**, 257 (1972).
[27] T. J. Pedley, *The Fluid Mechanics of Large Blood Vessels* (Cambridge University Press, Cambridge, England, 1980).